ACS APPLIED MATERIALS & INTERFACES

Research Article

www.acsami.org

Au@TiO_2–CdS Ternary Nanostructures for Efficient Visible-Light-Driven Hydrogen Generation

Jun Fang, Lin Xu, Zhenyi Zhang, Yupeng Yuan, Shaowen Cao, Zheng Wang, Lisha Yin, Yusen Liao, and Can Xue*

Solar Fuels Laboratory, School of Materials Science and Engineering, Nanyang Technological University, 50 Nanyang Avenue, Singapore 639798, Singapore

Supporting Information

ABSTRACT: We report a new type of Au@TiO_2–CdS ternary nanostructure by decorating CdS nanoparticles onto Au@TiO_2 core–shell structures. In comparison to that of binary structures such as CdS–TiO_2 and Au@TiO_2, these ternary nanostructures exhibit a remarkably high photocatalytic H_2-generation rate under visible-light irradiation. The enhanced photocatalytic activity is attributed to the unique ternary design, which builds up a transfer path for the photoexcited electrons of CdS to the core Au particles via the TiO_2 nanocrystal bridge and thus effectively suppresses the electron-hole recombination on the CdS photocatalyst. This internal electron-transfer pathway (CdS → TiO_2 → Au) eliminates the need for the postdeposition of the metal cocatalyst because the core Au nanoparticles can act as the interior active catalyst for proton reduction toward hydrogen evolution. We believe that our work demonstrates a promising way for the rational design of metal–semiconductor hybrid photocatalysts that can achieve a high photocatalytic efficiency for use in solar fuels production.

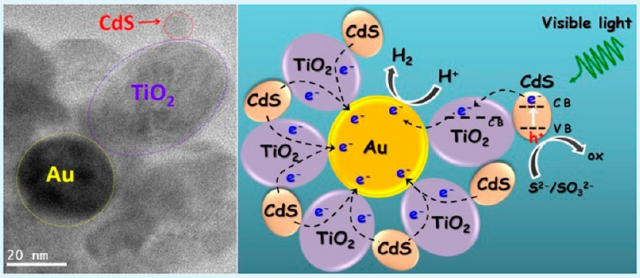

KEYWORDS: *Au particles, TiO_2, CdS, ternary nanostructure, H_2 generation, efficient electron transfer*

1. INTRODUCTION

Over the past decade, hydrogen fuel has been attracting more and more attention as a promising clean energy source as opposed to conventional fossil fuels.[1] Photocatalytic H_2 evolution over inorganic semiconductors under visible-light illumination has been widely explored as a potential avenue for solar fuels production.[2−4] In particular, TiO_2 has been extensively studied as one of the typical photocatalysts over the last few decades because of its low cost, nontoxicity, and high chemical stability.[5−8] However, the wide band gap (>3.2 eV) of TiO_2 restricts its utilization of the visible light in the solar spectrum, and the high recombination rate of photogenerated electrons and holes in TiO_2 often leads to a low quantum yield and poor photocatalytic activity.[9] Recent studies have demonstrated that combining a wide band-gap photocatalyst with smaller band-gap semiconductors, such as metal chalcogenides, would be an effective way to harvest visible light and promote charge separation, leading to a high photocatalytic efficiency for H_2 generation.[10−15] Among the small band-gap semiconductors, CdS is an excellent candidate because of its ideal band gap (2.4 eV) and band-edge levels that are capable of driving both the reduction and oxidation of water under visible-light irradiation. It has been reported that CdS–TiO_2 composites could show better photostability and photocatalytic activities than either individual component.[16−19]

Nevertheless, to apply the CdS–TiO_2 composites in the generation of H_2, the deposition of a noble-metal cocatalyst (e.g., Pt or Au) onto the composites is usually required to lower the overpotential for hydrogen evolution.[20−23] In general, the loading of metal cocatalysts allows rapid interfacial electron transfer from the excited semiconductors to the metal cocatalysts, which retards the recombination of photogenerated electron-hole pairs and thereby promotes photocatalytic efficiency. Conventionally, the postdeposition of metal nanoparticles onto semiconductor surfaces could be achieved through photodeposition or coprecipitation with calcination or reduction.[24] However, in the case of binary semiconductor composites (e.g., CdS–TiO_2), the postdeposition method usually leads to the random loading of metal nanoparticles onto the surfaces of both TiO_2 and CdS. Because the conduction band level of CdS is higher than that of TiO_2, in the visible-light-driven photocatalytic process of proton reduction into H_2, the photoexcited electrons in the CdS conduction band could rapidly transfer to the TiO_2 conduction band through the CdS–TiO_2 interfaces. As such, the effective proton reduction would have to occur on TiO_2 surfaces. To promote H_2 evolution on TiO_2 surface, it would be desirable to selectively deposit the metal cocatalysts on the TiO_2 surfaces rather than a random loading on CdS and TiO_2 surfaces in which the metal cocatalysts sitting on the CdS surfaces would become waste and may act as charge-recombination centers,

Received: June 4, 2013
Accepted: July 18, 2013
Published: July 18, 2013

   dx.doi.org/10.1021/am4021654 | ACS Appl. Mater. Interfaces 2013, 5, 8088–8092

decreasing the overall photocatalytic efficiency of CdS−TiO_2 composites.

Herein, we present the preparation of ternary Au@TiO_2−CdS nanostructures in which CdS nanoparticles are decorated on the outer surfaces of Au@TiO_2 core−shell structures. This rationally constructed ternary structure builds up a transfer path for the visible-light-excited electrons of CdS to the core Au particles via the TiO_2 nanocrystal bridge. This internal electron transfer pathway (CdS → TiO_2 → Au) eliminates the need for the postdeposition of metal cocatalyst because the core Au nanoparticle is not fully covered by the TiO_2 nanocrystal shell and thereby can act as the interior active cocatalyst for proton reduction toward hydrogen generation. As a result, this ternary Au@TiO_2−CdS structure exhibits significantly improved visible-light-driven activity for photocatalytic H_2 generation as compared to binary structures such as CdS−TiO_2 and Au@TiO_2. We believe that our study points to a promising way for the rational design of ternary nanostructures of metal−semiconductor hybrids that can achieve a high efficiency for use in photocatalytic solar fuels production.

2. EXPERIMENTAL SECTION

2.1. Sample Preparation. *Seed Growth of 40 nm Au Nanoparticles.* Fifteen nanometer Au nanoparticle seeds were synthesized by rapidly injecting an aqueous solution of trisodium citrate (5 mL, 38.8 mM) into a boiling aqueous solution of $HAuCl_4$ (50 mL, 1 mM) under vigorous stirring. After the solution color changed to deep-red, the heat source was removed to allow the solution to cool to room temperature. This solution is referred as the colloid of the 15 nm Au nanoparticle seeds. For the preparation of 40 nm Au nanoparticles, a typical procedure involved an aqueous solution of $HAuCl_4$ (125 mL, 0.25 mM) that was heated and kept boiling under vigorous stirring. Next, a 1.125 mL colloid solution of presynthesized 15 nm Au seeds and 0.56 mL of aqueous solution of sodium citrate (38.8 mM) were injected into the above solution. After the solution turned deep-red, a 5 mL solution of sodium citrate (38.8 mM) was added into the solution as the extra stabilizer, and the mixture was kept boiling for another 30 min.

Shell Growth of TiO_2 on the Au Nanoparticles. The growth of a TiO_2 nanocrystal shell on the 40 nm Au nanoparticles was achieved through a hydrothermal process according to literature protocols.[25] Typically, a 36 mL solution of the as-prepared 40 nm Au nanoparticles was mixed with 4.5 mL of an aqueous solution of TiF_4 (40 mM). The mixture was kept stirring for 30 min, diluted to 80 mL with deionized water, and transferred into a 100 mL Teflon-lined stainless steel autoclave that was subsequently held at 180 °C for 24 h. After that, the product was cooled to room temperature, centrifuged, and washed with deionized water several times.

Decorating CdS Nanoparticles onto Au@TiO_2 Core−Shell Structures. The calculated amount of $Cd(CH_3COO)_2{\cdot}2H_2O$ was added into 10 mL of an aqueous suspension of the Au@TiO_2 core−shell structures. Next, 50 μL of thioglycolic acid was added into the suspension under stirring. A stoichiometric amount of Na_2S was then introduced into the suspension. The suspension was transferred into a 40 mL Teflon-lined stainless steel autoclave that was subsequently held at 160 °C for 10 h. The product was cooled to room temperature, centrifuged, washed with deionized water several times, and air-dried at 60 °C. The final sample is denoted as Au@TiO_2−xCdS in which x refers to the molar ratio of CdS to TiO_2. (For instance, x = 0.1 means that CdS/TiO_2 is 10% in molar ratio.)

2.2. Sample Characterization. The crystalline phases of the samples were examined by powder X-ray diffraction (XRD) on a Shimazu XRD-6000 X-ray diffractometer (Cu Kα irradiation source) with a scanning speed of 2°/min in the 2θ range of 20−80°. UV−vis diffuse reflectance spectra were acquired on a Lambda 750 UV/vis/NIR spectrophotometer (PerkinElmer). The sample morphology was examined by field-emission scanning electron microscopy (SEM, JEOL JSM-7600F) with an energy-dispersive X-ray (EDX) analysis system and transmission electron microscopy (TEM, JEOL JEM-2010) with an accelerating voltage at 200 kV.

2.3. Photocatalytic Reduction of Water for H_2 Evolution. In a typical run, 2 mg of Au@TiO_2−xCdS photocatalysts was suspended in 10 mL of an aqueous solution containing 0.25 M Na_2S and 0.35 M Na_2SO_3 as the sacrificial agents. The suspension was sealed in a quartz vessel and purged with Argon for 30 min to drive away residual oxygen. After degassing, the vessel was exposed under a 300 W Xenon lamp (MAX-302, Asahi Spectra Company, Ltd.) coupled with a UV cutoff filter (λ >420 nm) to evaluate the photocatalytic activity under visible-light irradiation. The gas products were analyzed periodically by an Agilent 7890A gas chromatograph (GC) with a thermal conductivity detector (TCD). For the photocatalytic test under irradiation at a specific wavelength (420 or 550 nm), the experimental settings were identical to those described above except that the UV cutoff filter (λ >420 nm) was replaced with a band-pass filter (420 ± 10 or 550 ± 20 nm).

3. RESULTS AND DISCUSSION

The XRD patterns of Au@TiO_2 and various Au@TiO_2−CdS samples with different CdS-loading amounts are shown in Figure 1. For the Au@TiO_2 nanocomposite, we observed the

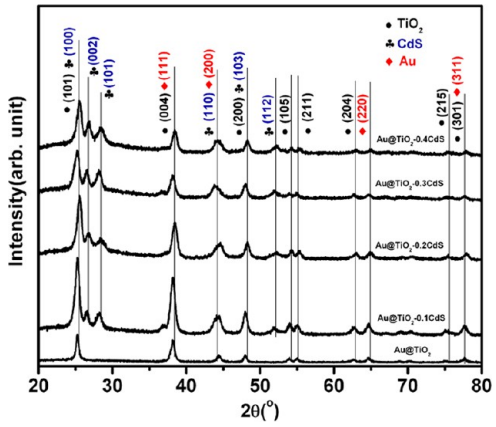

Figure 1. XRD patterns of various Au@TiO_2−CdS nanocomposites.

characteristic diffraction peaks of anatase TiO_2 (JCPDS card no. 83-2243) and face-centered cubic (FCC) Au (JCPDS card no. 01-1174). Note that the TiO_2 (004) peak at 38.2° is overlapping with the Au (111) peak at the same 2θ degrees. Upon decoration with CdS nanoparticles, the XRD patterns exhibit the characteristic peaks of hexagonal CdS (JCPDS card no. 41-4019). The CdS (110) peak at 43.9° has some overlap with the Au (200) peak at 44.4°. All peaks from the sample before CdS decoration remained present, indicating that the secondary-hydrothermal process did not influence the phases of the original Au@TiO_2 structures. In short, the final ternary structures contain three phases: FCC Au, anatase TiO_2, and hexagonal CdS.

The Au@TiO_2 core−shell structure was confirmed by TEM and SEM. As shown in Figure 2A,B, the 40 nm Au nanoparticles were all encapsulated in TiO_2 nanocrystal shells, forming flowerlike spherical structures with an average diameter of ~120 nm. The molar ratio of Au to TiO_2 was estimated to be ~5% according to EDX analysis (Figure S2). After the secondary-hydrothermal process for CdS decoration, such flowerlike structures were well preserved, as shown in Figures 2C,D and S1. We observed CdS nanoparticles (10−20 nm) appearing on the outer surface of the TiO_2 nanocrystal shells,

dx.doi.org/10.1021/am4021654 | ACS Appl. Mater. Interfaces 2013, 5, 8088−8092

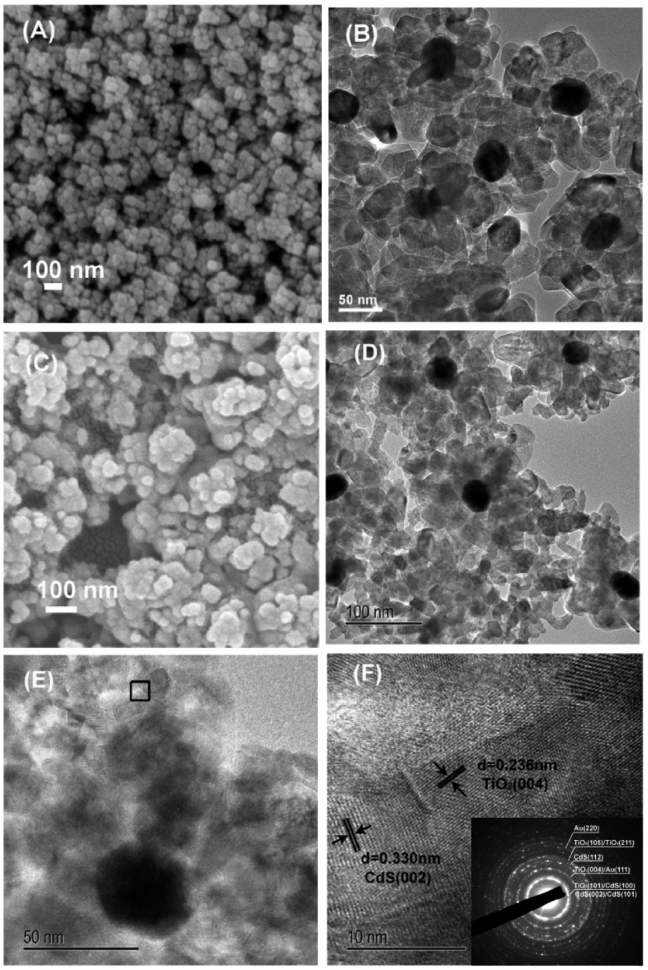

Figure 2. SEM and TEM images of the as-prepared Au@TiO_2−CdS nanocomposites. (A) SEM image of Au@TiO_2. (B) TEM image of Au@TiO_2. (C) SEM image of Au@TiO_2−0.2CdS. (D, E) TEM images of Au@TiO_2−0.2CdS. (F) HRTEM image of Au@TiO_2−0.2CdS. The inset of panel F is the SAED patterns of Au@TiO_2−0.2CdS.

and the density of the CdS particles increased as the ratio of CdS to TiO_2 increased. EDX analysis (Figure S2) confirmed that for all Au@TiO_2−xCdS samples the actual CdS to TiO_2 ratio is fairly close to the theoretically calculated ratio on the basis of the precursor concentrations. The HRTEM images (Figure 2E,F) reveal that the CdS nanoparticles are intimately contacted with the TiO_2 nanocrystal shells with clear CdS−TiO_2 interfaces. In Figure 2F, we observed a lattice spacing of 0.236 nm corresponding to the (004) facet of anatase TiO_2 and another lattice spacing of 0.330 nm corresponding to the (002) facet of hexagonal CdS. The selected area electron diffraction (SAED) pattern is shown in the inset of Figure 2F. The labels from the lower position to the upper positions are TiO_2(101)/CdS(100)/CdS(002)/CdS(101), TiO_2(004)/Au(111), CdS-(112), TiO_2(105)/TiO_2(211), and Au(220), respectively, which is in agreement with the XRD results.

Figure 3 shows the absorption spectra of the Au@TiO_2−xCdS ternary nanostructures. The UV absorption band at ~320 nm could be attributed to the band-edge absorption of anatase TiO_2.[26] The absorption features from 360 to 520 nm arise from the band absorption of CdS nanoparticles.[27] On the basis of the XRD results, the crystalline sizes of the CdS particles were calculated as 12.1, 8.27, 12.0, and 10.0 nm for Au@TiO_2−

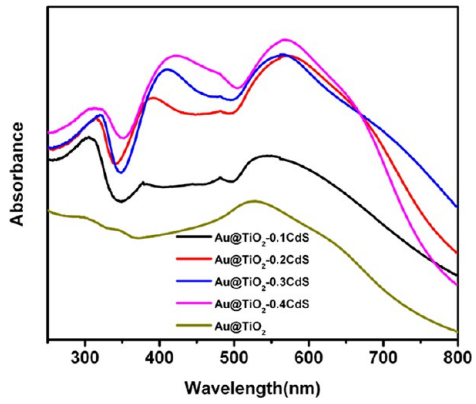

Figure 3. UV−vis diffuse reflectance spectra of various Au@TiO_2−CdS samples.

0.1CdS, Au@TiO_2−0.2CdS, Au@TiO_2−0.3CdS, and Au@TiO_2−0.4CdS, respectively. Moreover, this CdS absorption band red shifts with higher loading amounts of CdS, which might be due to the aggregation of the CdS nanoparticles into larger domains.[27] The absorption features from 530 to 580 nm come from the surface plasmon resonance (SPR) characteristic of the 40 nm Au nanoparticles encapsulated in the TiO_2 shells.[8]

It is notable that the Au SPR absorption peak shows a red shift from 530 nm (Au@TiO_2) to 570 nm (Au@TiO_2−0.4CdS). This implies that in the Au@TiO_2 core−shell structure, the TiO_2 nanocrystalline shell may not fully cover the entire surface of the Au nanoparticle core; thus, in the hydrothermal process of CdS decoration on the Au@TiO_2 structure, some CdS could directly deposit on the Au nanoparticle surface,[29] as evidenced by the HRTEM observation (Figure S3). It is well known that the SPR wavelength of a Au nanoparticle is highly sensitive to the dielectric environment near its surface;[30] as such, the higher dielectric constant of CdS (vs air) and the direct contact of the deposited CdS with the Au nanoparticle surface would lead to a red shift of the Au SPR band. To further verify this hypothesis, we performed an etching treatment on the Au@TiO_2−0.2CdS sample using an HCl solution to remove the deposited CdS. The absorption spectra (Figure S4) showed that the peak attributed to CdS was attenuated sharply and the SPR wavelength of the Au nanoparticles retreated from 570 nm to 545 nm after HCl etching. This confirms the influence of the deposited CdS on the Au SPR absorption features.

The ternary Au@TiO_2−xCdS nanostructures were used for photocatalytic H_2 generation under visible-light (λ >420 nm) irradiation in an aqueous electrolyte solution containing 0.25 M Na_2S and 0.35 M Na_2SO_3, which act as the sacrificial agents to quench the holes. Control samples of pure CdS nanoparticles and the TiO_2−0.2CdS nanocomposite without Au cores were also prepared for comparison. (See the Supporting Information for details.) As shown in Figure 4, we observed very weak photocatalytic activity in H_2 generation for both the pure CdS (0.25 μmol h^{-1}) and TiO_2−0.2CdS (0.28 μmol h^{-1}) samples. Significantly, in the presence of Au nanoparticle cores, the ternary Au@TiO_2−0.2CdS sample exhibited a more than 10-fold higher activity (3.94 μmol h^{-1}) as compared to the TiO_2−0.2CdS sample without Au cores. The remarkable enhancement in photocatalytic activity could be attributed to the unique design of the ternary Au@TiO_2−CdS structures that allow for an efficient CdS → TiO_2 → Au pathway for electron transfer, as illustrated in Figure 5. Upon light excitation, active electrons

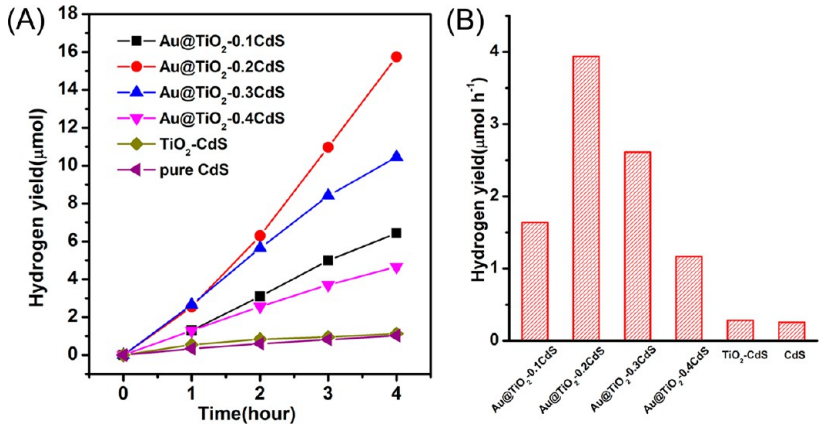

Figure 4. (A) Plots of the photocatalytic H_2-evolution amount versus visible-light-irradiation (λ >420 nm) time by various samples. (B) H_2-evolution rate by various samples.

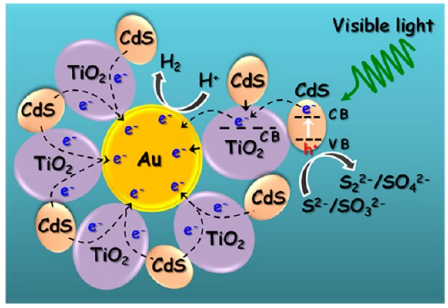

Figure 5. Schematic illustration of photocatalytic H_2 generation by Au@TiO_2–CdS ternary nanostructures under visible-light irradiation.

are generated in the CdS conduction band and then are rapidly injected into the conduction band of the contacted TiO_2, which serves as a bridge to transport these electrons to the Au core. It is known that the Au nanoparticle can act as electron trap in the photocatalytic process to promote the separation of photogenerated charge carriers.[31] Therefore, the Au cores in this ternary structure could capture and store the photoexcited electrons from CdS nanoparticles on the TiO_2 shells to induce the proton reduction for H_2 evolution on the Au surface, whereas the photogenerated holes remaining on CdS could be quenched by the sulfide ions in the solution. It is believed that this internal (CdS → TiO_2 → Au) electron-transfer process effectively suppressed the electron-hole recombination on CdS and thereby significantly enhanced the photocatalytic H_2-generation rate.

A direct contribution of photocatalytic activity from Au SPR excitation could be excluded because the Au@TiO_2 core–shell sample before CdS decoration showed an extremely low H_2-generation rate (0.001 μmol h^{-1}, not shown in Figure 4 because it is too low). This suggests that the CdS nanoparticles could be considered as the sole visible-light absorber to induce photocatalytic activity. Consistently, we observed a 2.4-fold increased H_2-generation rate when the CdS-loading ratio increases from that of the Au@TiO_2–0.1CdS sample (1.64 μmol h^{-1}) to the Au@TiO_2–0.2CdS sample (3.94 μmol h^{-1}). However, it was found that further increasing the CdS decoration amount led to lower photocatalytic activity, which is evidenced by the decreased H_2-generation rate for the Au@TiO_2–0.3CdS sample (2.61 μmol h^{-1}) and the Au@TiO_2–0.4CdS sample (1.16 μmol h^{-1}). This could be attributed to two reasons. First, the overloading of CdS onto Au@TiO_2 structures might retard the proton diffusion through the internal vacancies within the ternary structure, which could reduce the photocatalytic activity of proton reduction. Second, the higher precursor concentration for more CdS loading might result in the aggregation of CdS nanoparticles on the TiO_2 shells, as evidenced by Figure S1F, and such an aggregation of CdS particles could create grain boundaries that would trap charge carriers during the charge-transfer process to decrease the photocatalytic reactions.

It has been reported that SPR of Au nanoparticles could also enhance the charge separation of nearby semiconductors through plasmon-exciton coupling and thereby promote photocatalytic performance.[28] For our ternary Au@TiO_2–CdS structures, to test whether the SPR of Au cores contributes to the enhanced H_2-generation rate we carried out additional photocatalytic tests using the Au@TiO_2–0.2CdS sample while controlling the irradiation wavelengths. In a control experiment, under light irradiation at 420 ± 10 nm, which excites only CdS nanoparticles, there was apparent H_2 evolution with a rate of 0.1 μmol h^{-1} (corresponding to a quantum yield of 0.55%). However, when we simultaneously introduced a secondary irradiation at 550 ± 20 nm, which excites the SPR of Au cores, no enhancement of the H_2-generation rate was observed. This means that the SPR excitation of Au cores could not provide a significant contribution to the photocatalytic activity of the ternary Au@TiO_2–CdS nanostructures.

The stability of the photocatalyst was also evaluated through a recycling test of photocatalytic H_2 evolution using the Au@TiO_2–0.2CdS structure. As shown in Figure S6, after three cycles the photocatalytic H_2-generation rate can still maintain 90% of the original activity as compared to the first cycle, suggesting a good stability of Au@TiO_2–0.2CdS. Nevertheless, the 10% drop in activity suggests that photocorrosion of CdS particles may still occur during the photocatalytic reactions.

4. CONCLUSIONS

Ternary Au@TiO_2–CdS nanostructures were successfully constructed through the decoration of CdS nanoparticles onto Au@TiO_2 core–shell structures. This ternary design builds up a transfer path for the photoexcited electrons of CdS to the core Au particles via the TiO_2 nanocrystal bridge and thus effectively suppresses the electron-hole recombination on the CdS photocatalyst. As such, these ternary nanostructures exhibit a remarkably high photocatalytic H_2-generation rate under visible-light irradiation compare to that of binary

dx.doi.org/10.1021/am4021654 | ACS Appl. Mater. Interfaces 2013, 5, 8088–8092

structures such as CdS−TiO_2 and Au@TiO_2. This internal electron-transfer pathway (CdS → TiO_2 → Au) eliminates the needs for the postdeposition of the metal cocatalyst because the core Au nanoparticle can act as the interior active cocatalyst for proton reduction toward hydrogen evolution. We believe that our work demonstrates a promising way for the rational design of metal−semiconductor hybrid photocatalysts that can achieve a high photocatalytic efficiency for use in solar fuels production.

■ ASSOCIATED CONTENT

Supporting Information

Methods for the synthesis of CdS nanoparticles and TiO_2−0.2CdS nanocomposite without Au cores and for etching CdS nanoparticles to reobtain the Au@TiO_2 core−shell structure. SEM and TEM images of as-prepared Au@TiO_2−CdS nanocomposites, EDX analysis of various Au@TiO_2−CdS nanocomposites, UV−vis diffuse reflectance spectra of Au@TiO_2−0.2CdS before and after 3 M HCl etching, TEM images of TiO_2−0.2CdS and pure CdS catalysts, recycling photocatalytic H_2-evolution test using Au@TiO_2−0.2CdS, and the band-energy diagram for the Au@TiO_2−CdS ternary structure. This material is available free of charge via the Internet at http://pubs.acs.org.

■ AUTHOR INFORMATION

Corresponding Author

*Tel: +65-6790 6180. E-mail: cxue@ntu.edu.sg.

Notes

The authors declare no competing financial interest.

■ ACKNOWLEDGMENTS

This work is financially supported by a NTU start-up grant (SUG), NTU seed funding for the Solar Fuels Laboratory, MOE AcRF-Tier1 RG 44/11, MOE AcRF-Tier 2 (MOE2012-T2-2-041, ARC 5/13), and CRP (NRF-CRP5-2009-04) from NRF Singapore.

■ REFERENCES

(1) Penner, S. S. *Energy* **2006**, *31*, 33−43.
(2) Chen, X. B.; Shen, S. H.; Guo, L. J.; Mao, S. S. *Chem. Rev.* **2010**, *110*, 6503−6570.
(3) Kudo, A.; Miseki, Y. *Chem. Soc. Rev.* **2009**, *38*, 253−278.
(4) Kubacka, A.; García, M. F.; Colón, G. *Chem. Rev.* **2012**, *112*, 1555−1614.
(5) Fujishima, A.; Honda, K. *Nature* **1972**, *238*, 37−38.
(6) Thompson, T. L.; Yates, J. T. *Chem. Rev.* **2006**, *106*, 4428−4453.
(7) Antony, R. P.; Mathews, T.; Ramesh, C.; Murugesan, N.; Dasgupta, A.; Dhara, S.; Dash, S.; Tyagi, A. K. *Int. J. Hydrogen Energy* **2012**, *37*, 8268−8276.
(8) Fang, J.; Cao, S. W.; Wang, Z.; Shahjamali, M. M.; Boey, F.; Loo, S. C. J.; Barber, J.; Xue, C. *Int. J. Hydrogen Energy* **2012**, *37*, 17853−17861.
(9) Asahi, R.; Morikawa, T.; Ohwaki, T.; Aoki, K.; Taga, Y. *Science* **2001**, *293*, 269−271.
(10) Yin, M.; Wu, C. K.; Lon, Y. B.; Burda, C.; Koberstein, J. T.; Zhu, Y. M.; ÓBrien, S. *J. Am. Chem. Soc.* **2005**, *127*, 9506−9511.
(11) Song, W.-S.; Yang, H. *Chem. Mater.* **2012**, *24*, 1961−1967.
(12) Hameed, A.; Montini, T.; Gamboa, V.; Fornasiero, P. *J. Am. Chem. Soc.* **2008**, *130*, 9658−9659.
(13) Kamat, P. V. *J. Phys. Chem. C* **2007**, *111*, 2834−2860.
(14) Gupta, S. M.; Tripathi, M. *High Energy Chem.* **2012**, *46*, 1−9.
(15) Wu, L.; Yu, J. C.; Fu, X. Z. *J. Mol. Catal.* **2006**, *244*, 25−32.
(16) Li, G. S.; Zhang, D. Q.; Yu, J. C. *Environ. Sci. Technol.* **2009**, *43*, 7079−7085.
(17) Xie, Y.; Ali, G.; Yoo, S. H.; Cho, S. O. *ACS Appl. Mater. Interfaces* **2010**, *2*, 2910−2914.
(18) Xia, Y.; Tang, Z. *Chem. Commun.* **2012**, *48*, 6320−6336.
(19) Li, J. T.; Hoffmann, M. W. G.; Shen, H.; Fabrega, C.; Prades, J. D.; Andreu, T.; Ramirez, F. H.; Mathur, S. *J. Mater. Chem.* **2012**, *22*, 20472−20476.
(20) Jang, J. S.; Choi, S. H.; Kim, H. G.; Lee, J. S. *J. Phys. Chem. C* **2008**, *112*, 17200−17205.
(21) Park, H.; Choi, W. Y.; Hoffmann, M. R. *J. Mater. Chem.* **2008**, *18*, 2379−2385.
(22) Ye, M.; Gong, J. J.; Lai, Y. K.; Lin, C. J.; Lin, Z. Q. *J. Am. Chem. Soc.* **2012**, *134*, 15720−15723.
(23) Park, H.; Kim, Y. K.; Choi, W. *J. Phys. Chem. C* **2011**, *115*, 6141−6148.
(24) Reber, J. F.; Rusek, M. *J. Phys. Chem.* **1986**, *90*, 824−834.
(25) Wu, X. F.; Song, H. Y.; Yoon, J. M.; Yu, Y. T.; Chen, Y. F. *Langmuir* **2009**, *25*, 6438−6447.
(26) Zhang, N.; Liu, S. Q.; Fu, X. Z.; Xu, Y. J. *J. Phys. Chem. C* **2011**, *115*, 9136−9145.
(27) Baker, D. R.; Kamat, P. V. *Adv. Funct. Mater.* **2009**, *19*, 805−811.
(28) Cao, S. W.; Yin, Z.; Barber, J.; Boey, F.; Loo, S. C. J.; Xue, C. *ACS Appl. Mater. Interfaces* **2012**, *4*, 418−423.
(29) Tada, H.; Mitsui, T.; Kiyonaga, T.; Akita, T.; Tanaka, K. *Nat. Mater.* **2006**, *5*, 782−786.
(30) Kelly, K. L.; Coronado, E.; Zhao, L. L.; Schatz, G. C. *J. Phys. Chem. B* **2003**, *107*, 668−677.
(31) Silva, C. G.; Juárez, R.; Marino, T.; Molinari, R.; García, H. *J. Am. Chem. Soc.* **2011**, *133*, 595−602.